SCIENCE CHINA
Life Sciences

•RESEARCH PAPER•

November 2023 Vol.66 No.11: 2646–2662
https://doi.org/10.1007/s11427-022-2330-4

Calcium-dependent protein kinases CPK21 and CPK23 phosphorylate and activate the iron-regulated transporter IRT1 to regulate iron deficiency in *Arabidopsis*

Zhangqing Wang[1†], Yanting Zhang[1†], Yisong Liu[1], Dali Fu[1], Zhang You[1], Panpan Huang[1], Huiling Gao[1], Zhenqian Zhang[1] & Cun Wang[1,2*]

[1]*State Key Laboratory of Crop Stress Biology for Arid Areas and College of Life Sciences, Northwest A&F University, Yangling 712100, China;*
[2]*Institute of Future Agriculture, Northwest Agriculture & Forestry University, Yangling 712100, China*

Received December 16, 2022; accepted March 15, 2023; published online June 5, 2023

Iron (Fe) is an essential micronutrient for all organisms. Fe availability in the soil is usually much lower than that required for plant growth, and Fe deficiencies seriously restrict crop growth and yield. Calcium (Ca^{2+}) is a second messenger in all eukaryotes; however, it remains largely unknown how Ca^{2+} regulates Fe deficiency. In this study, mutations in *CPK21* and *CPK23*, which are two highly homologous calcium-dependent protein kinases, conferredimpaired growth and rootdevelopment under Fe-deficient conditions, whereas constitutively active CPK21 and CPK23 enhanced plant tolerance to Fe-deficient conditions. Furthermore, we found that CPK21 and CPK23 interacted with and phosphorylated the Fe transporter IRON-REGULATED TRANSPORTER1 (IRT1) at the Ser149 residue. Biochemical analyses and complementation of Fe transport in yeast and plants indicated that IRT1 Ser149 is critical for IRT1 transport activity. Taken together, these findings suggest that the CPK21/23-IRT1 signaling pathway is critical for Fe homeostasis in plants and provides targets for improving Fe-deficient environments and breeding crops resistant to Fe-deficient conditions.

***Arabidopsis*, calcium-dependent protein kinases, IRT1, iron**

Citation: Wang, Z., Zhang, Y., Liu, Y., Fu, D., You, Z., Huang, P., Gao, H., Zhang, Z., and Wang, C. (2023). Calcium-dependent protein kinases CPK21 and CPK23 phosphorylate and activate the iron-regulated transporter IRT1 to regulate iron deficiency in *Arabidopsis*. Sci China Life Sci 66, 2646–2662. https://doi.org/10.1007/s11427-022-2330-4

INTRODUCTION

Iron (Fe) is essential for the normal growth of all plants and is an important regulator of a variety of cellular processes involved in chlorophyll biosynthesis, photosynthesis, and respiration (Connolly et al., 2002; Vert et al., 2002). Fe deficiency in animals and plants causes serious diseases, including anemia and plant chlorosis, respectively (Briat et al., 1995; Kobayashi and Nishizawa, 2012). Although soil is rich in Fe, most Fe exists in the form of insoluble ferric complexes; hence, Fe deficiencies are a more widely spread problem in alkaline and calcareous soils (Eide et al., 1996; Guerinot and Yi, 1994). Non-grass plants, such as *Arabidopsis*, acidify the rhizosphere and reduce Fe(III) to Fe(II) via Fe(III) chelate reductase (FRO2). Then, Fe(II) is transported into root cells by IRON-REGULATED TRANSPORTER1 (IRT1), and IRT1 is responsible for Fe uptake under Fe-deficient conditions (Marschner and Römheld, 1994; Robinson et al., 1999; Vert et al., 2002).

Recent studies have shown that AtIRT1 is a multi-transmembrane protein that appears on the *trans*-Golgi network/early endosome (TGN/EE) and cycles between TGN/EE and the plasma membrane (PM); this cycle is regulated

†Contributed equally to this work
*Corresponding author (email: cunwang@nwafu.edu.cn)

by the secondary substrates Zn, Mn, and Co but not Fe (Barberon et al., 2014; Barberon et al., 2011). The IRT1 Fe uptake mechanism in roots is tightly regulated at the transcriptional and post-transcriptional levels to meet the demand for Fe (Brumbarova et al., 2015; Connolly et al., 2002). As the central transcriptional factor involved in Fe uptake, FIT is essential for high-level induction of the *AHA2*, *FRO2*, and *IRT1* genes (Brumbarova et al., 2015; Colangelo and Guerinot, 2004; Ivanov et al., 2012; Jakoby et al., 2004). In addition, ENHANCED BENDING1 (EHB1), which is a Ca^{2+}-dependent IRT1 inhibitor, is a negative regulator of Fe acquisition (Gratz et al., 2021; Khan et al., 2019).

Several factors that control IRT1 post-translational modification have emerged recently, and IRT1 has been used as a model plant PM protein to study the complex mechanism of plant endocytosis (Barberon et al., 2014; Barberon et al., 2011; Ivanov et al., 2014; Shin et al., 2013). Ubiquitin (Ub)-mediated endocytosis of IRT1 is a key mechanism controlling IRT1 distribution and Fe uptake by cells. Under excess nonferrous metal conditions, ultimonoUb is triggered to extend to the K63 polyUb chain, and the large cytosolic loop of the IRT1 transporter is phosphorylated by CBL-interacting protein kinase CIPK23 as a sensor; in turn, this phosphorylation creates a docking site that promotes the recruitment of IDF1 E3 Ub ligase, which facilitates direct IRT1 degradation, thereby regulating the stability of the intracellular IRT1 protein (Dubeaux et al., 2018; Shin et al., 2013). In addition, hormones, including gibberellin (GA), nitric oxide (NO), and ethylene, are involved in the Fe-response signaling pathway (Lingam et al., 2011; Meiser et al., 2011; Wild et al., 2016). For example, when Fe is abundant, the GA signaling DELLA repressor directly binds to FIT, thereby inhibiting the expression of the downstream IRT1 gene (Wild et al., 2016).

Ca^{2+} is the most important second messenger in signal transduction and plays an important role in the regulation of plant development and stress response (Dong et al., 2021; Luan and Wang, 2021). When plants are subjected to stressful stimuli, transient changes in intracellular Ca^{2+} concentration cause specific calcium signals, receptor recognition, and perception, which, in turn, translate into transcriptional and metabolic responses (Boudsocq and Sheen, 2013; Hashimoto and Kudla, 2011; Perochon et al., 2011). In this regard, calcium-dependent protein kinases (CPKs) are important calcium regulatory proteins commonly found when deciphering Ca^{2+} signals triggered by impaired development and multiple stress stimuli (Hamel et al., 2014; Liu et al., 2017). CPKs are serine/threonine (Ser/Thr) protein kinases that are directly activated by Ca^{2+} signals. Thus far, 34 CPKs have been reported in *Arabidopsis*, which occur in various organs and widely participate in the regulation of growth and development as well as in the stress response (Brandt et al., 2012; Harmon et al., 2001; Valmonte et al., 2014; Wang et al., 2016; Zhou et al., 2014; Zhu et al., 2007). However, it has not been reported whether CPKs participate in regulating plant tolerance to Fe-deficient conditions.

In this study, the calcium-dependent protein kinases CPK21 and CPK23 recognized the Ca^{2+} signals induced by Fe-deficient conditions. The *cpk21/23* mutant presented impaired root length and fresh weight under Fe-deficient conditions, whereas the constitutively active *Arabidopsis* plants (*CPK21-CA* and *CPK23-CA*) exhibited enhanced tolerance to Fe-deficient conditions. We determined that CPK21 or CPK23 interacts and phosphorylates IRT1 primarily at the Ser149 residue. Activated IRT1 transports Fe^{2+} from outside of the plant into the cytoplasm, which increases tolerance to Fe deficiency. Taken together, these findings reveal that the CPK21/23-IRT1 signaling pathway is a key mechanism for establishing plant resilience to Fe-deficient conditions and reveals how plants initiate their adaptive responses to Fe micronutrient deficiency.

RESULTS

CPK21 and CPK23 are required under Fe-deficient conditions

To explore whether CPKs are involved in Fe deficiency signaling and which CPKs are involved in regulation, we tested 33 *cpk* single mutants available in our laboratory in a Fe deficiency phenotype assay. No differences were detected between these *cpk* single mutants and the wild-type (WT) (Figure S1A–C in Supporting Information). Since then, studies have shown redundancy and specificity between CPK isoforms (Gutermuth et al., 2018; Liu et al., 2017; Prodhan et al., 2018; Zhou et al., 2020). Therefore, based on the evolutionary protein sequence alignment (Liu et al., 2017), we used a multiple mutant approach and obtained 12 multiple mutants by crossing to analyze the Fe deficiency phenotype. CPK21 loss-of-function alleles were introduced into *cpk23* or *cpk15/23* mutants by CRISPR/Cas-mediated mutagenesis, resulting in *cpk21/23* double mutants and *cpk15/21/23* triple mutants (Fu et al., 2022). Interestingly, among the mutants generated, the *cpk15/21/23* and *cpk21/23* mutants exhibited distinct Fe deficiency phenotypes, including reduced primary root length and biomass (Figure S2G–I in Supporting Information), whereas the other multiple mutants did not exhibit these phenotypes (Figure S2A and D in Supporting Information). The *cpk21/23* and *cpk15/21/23* mutants showed the same trend, suggesting that deleting *CPK21* and *CPK23*, rather than deleting *CPK15*, was responsible for the increased sensitivity in the plants.

Because *cpk21/23* was created using CRISPR/Cas-mediated mutagenesis, two lines of the *cpk21/23* double mutant were subjected to Fe deficiency phenotype analysis with *irt1* as the control to further determine the Fe deficiency phe-

notype of the *cpk21*/*23* mutant. The results showed that both *cpk21*/*23* double mutant lines exhibited a sensitive phenotype, whereas *irt1* exhibited an extremely sensitive phenotype, including shorter root length and reduced fresh weight (Figure 1A–C). Our reverse genetic phenotypic analysis of the *cpk21*, *cpk23*, and *cpk21*/*23* double mutants revealed the consequences of the collective loss of CPK function under Fe-deficient conditions but failed to reveal a single contribution of CPK21 or CPK23 to iron biology. Therefore, to further evaluate the specific roles of CPK21 and CPK23 in Fe-deficient stress, we designed a complementary genetic approach to independently overexpress these two kinases.

Thus, we introduced the *CPK21* or *CPK23* coding sequence into the pCAMBIA1307-FLAG vector under the control of the *CaMV35S* promoter and created *Arabidopsis* plants overexpressing *CPK21* or *CPK23* (*CPK21-OE* and *CPK23-OE*). Under Fe-deficient conditions, the root length and fresh weight of *CPK21-OE* and *CPK23-OE* were not significantly different from those of the WT (Figure S3A and C in Supporting Information). To determine why the overexpressed plants had no phenotype, we measured the expression levels of *CPK21* and *CPK23* in the overexpressed plants. The results showed that these genes were overexpressed approximately two-fold, which was not as high as expected (Figure S3E and F in Supporting Information). Studies have shown that the N-terminal EF-hand of CPK21 is activated only at very high Ca^{2+} concentrations, whereas CPK23 is fully activated at basal Ca^{2+} concentrations (Geiger et al., 2010; Scherzer et al., 2012; van Kleeff et al., 2018). We speculated that the change in CPK21 activity may contribute to Fe-deficient conditions, rather than the expression level of CPK21, and that overexpression of *CPK23* is not high enough to cause a significant difference. CPKs contain a variable N-terminal domain followed by a Ser/Thr protein kinase domain and an autoinhibitory junction domain (JD) that is connected with the C-terminal CaM-like regulatory domain (CaMLD) via a chain (Yip Delormel and Boudsocq, 2019). Therefore, we removed the JD and CaMLD domains of the kinase and introduced the *CPK21* or *CPK23* sequence into the pCAMBIA1307-FLAG vector to obtain *CPK21* or *CPK23* constitutively active *Arabidopsis* plants (*CPK21-CA* and *CPK23-CA*) (Figure S4B and D in Supporting Information). As a result, the root growth and fresh weights of the three *CPK21-CA* lines increased significantly under Fe-deficient conditions, compared with those of the WT (Figure 1D–F), and the three *CPK23-CA* lines also shared this phenotype (Figure 1G–I).

Next, quantitative reverse transcription-polymerase chain reaction (qRT-PCR) analysis was performed to explore whether the CPK21 and CPK23 expression levels were induced by Fe-deficient conditions. As a result, the *CPK21* and *CPK23* expression levels peaked at 3 h of treatment (Figure S3G in Supporting Information), indicating that *CPK21* and *CPK23* respond to Fe-deficient signaling and are most likely redundant.

CPK21 and CPK23 interact with the IRT1 transporter

Next, we compared the co-expression of IRT1, CPK21, and CPK23, a necessary prerequisite for physiologically meaningful interaction. We observed a common distribution of these proteins on the PM of the roots in the Fe deficiency-treated 5-day-old *ProIRT1*:*IRT1*-GFP, *ProCPK21*:*CPK21*-GFP, and *ProCPK23*:*CPK23*-GFP transgenic lines (Figure S5A and B in Supporting Information). Histochemical analysis of GUS activity in *ProIRT1*:*GUS*, *ProCPK21*:*GUS*, and *ProCPK23*:*GUS* transgenic plants treated under Fe-deficient conditions showed that they were all stained in the roots (Figure S5C and D in Supporting Information), which was consistent with previous reports (Franz et al., 2011; Ma and Wu, 2007; Vert et al., 2002). These results suggest that the subcellular localization and tissue expression patterns of IRT1, CPK21, and CPK23 are the same under Fe-deficient conditions.

To examine whether CPK21 and CPK23 interact with IRT1, a bimolecular fluorescence complementation (BiFC) assay was performed to examine the possible interactions between CPK21, CPK23, and IRT1. CBL1-OFP was used as the PM marker (D'Angelo et al., 2006). We also used CPK15, another member of the CPK family with the closest protein sequence to CPK21 and CPK23. When CPK21-nYFP or CPK23-nYFP was co-expressed with IRT1-cYFP, strong fluorescence signals were observed, and the YFP signals co-localized with the PM marker. No fluorescence was detected when CPK15-nYFP, CPK21-nYFP, or CPK23-nYFP was co-expressed with the β-glucuronidase gene fused to cYFP (GUS-cYFP; control) or when IRT1-cYFP was co-expressed with GUS-nYFP (Figure 2A). These findings suggest that CPK21 and CPK23 interacted with IRT1 at the PM, whereas CPK15 did not interact with IRT1. To determine whether the interaction took place on the PM, we used Fiji/ImageJ to analyze the fluorescence signals and determined that the fluorescence peaks of the YFP and PM markers overlapped (Figure 2B).

To confirm the BiFC assay results, we performed a luciferase complementation imaging (LCI) assay. The results showed that LUC activity was detected when CPK21-nLUC or CPK23-nLUC was co-expressed with IRT1-cLUC but not CPK15-nLUC. In contrast, co-expression of CPK15/CPK21/CPK23-nLUC or IRT1-cLUC with the negative controls GUS-cLUC or GUS-nLUC did not produce LUC activity (Figure 2C).

A glutathione S-transferase (GST) pull-down assay was performed to verify the interaction between CPK21/CPK23 and IRT1. The full-length IRT1 fused to GST could not be purified in our system, so we constructed an intracellular

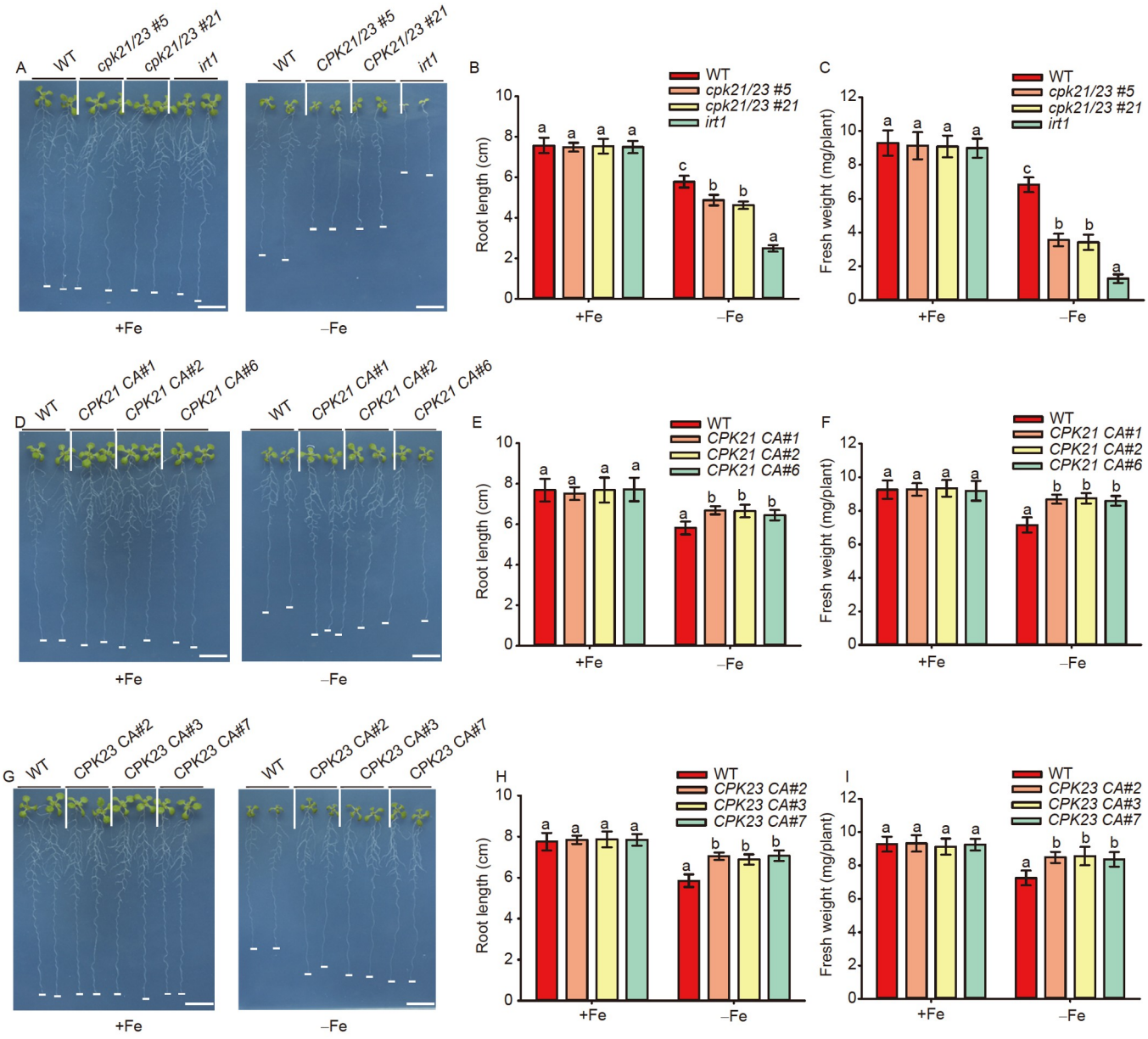

Figure 1 Phenotypic analysis of the mutants and constitutively active plants. A, Fe deficiency phenotypes of *cpk21/23* mutants. Scale bars, 1 cm. B, Statistical analysis of the root lengths of the plants shown in (A). C, Statistical analysis of the fresh weights of the plants shown in (A). D, Fe deficiency phenotypes of the *CPK21-CA* plants. Scale bars, 1 cm. E, Statistical analysis of the root lengths of the plants shown in (D). F, Statistical analysis of the fresh weights of the plants shown in (D). G, Fe deficiency phenotypes of *CPK23-CA* plants. Scale bars, 1 cm. H, Statistical analysis of the root lengths of the plants shown in (G). I, Statistical analysis of the fresh weights of the plants shown in (G). Data are presented as mean±SD (n=15 seedlings/genotype).

IRT1 fragment fused to a GST tag (IRT1vr; amino acid residues 144–192). Interactions were most likely to occur, as this fragment is long and contains the most phosphorylation sites, whereas other fragments either contain one/no phosphorylation sites or are located on the other side of the PM. We incubated the CPK15/CPK21/CPK23-His-tagged proteins with GST-IRT1vr or GST alone. CPK21/CPK23-His was pulled down by GST-IRT1vr but not by GST alone, whereas CPK15-His was not pulled down by GST-IRT1vr or GST. The results of these pull-down assays show that CPK21 and CPK23 interacted directly with IRT1vr (Figure 2D).

To further study whether CPK21/CPK23 interacted with IRT1 *in vivo*, a co-immunoprecipitation (Co-IP) assay was performed. We crossed *ProIRT1*:IRT1-3xFLAG or *Pro35S*:GUS-3xFLAG with *ProCPK21*:CPK21-GFP, *ProCPK23*:CPK23-GFP, or *Pro35S*:GFP plants to obtain transgenic lines. In *ProIRT1*:IRT1-3xFLAG/*ProCPK21*:CPK21-GFP or *ProIRT1*:IRT1-3xFLAG/*ProCPK23*:CPK23-GFP transgenic plants, IRT1 was effectively immunoprecipitated by CPK21 or CPK23, whereas IRT1 was not detected in IP samples from other transgenic plants (Figure 2E). Taken together, these results indicate that CPK21 and CPK23 in-

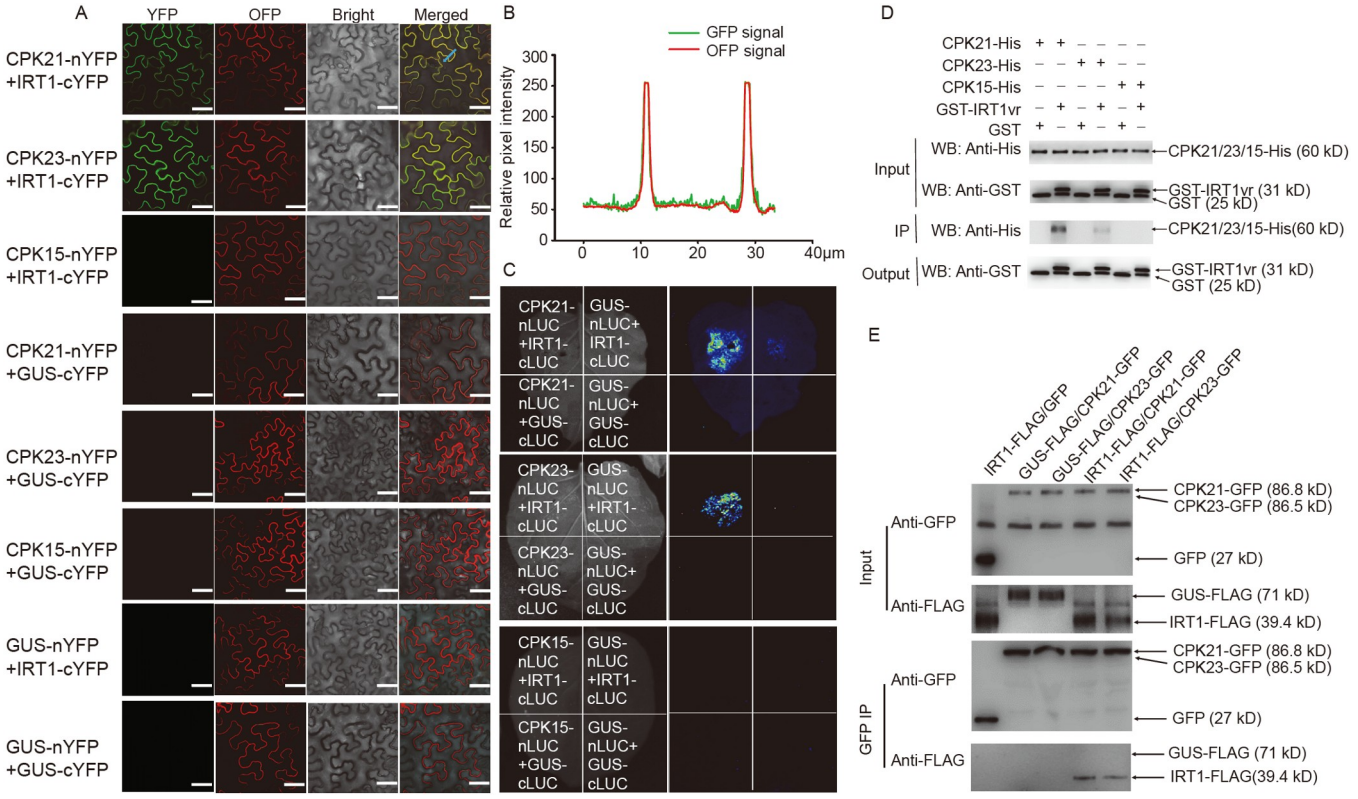

Figure 2 CPK21 and CPK23 physically interact with IRT1. A, BiFC assay showing the interaction between CPK21/CPK23/CPK15 and IRT1. CPK21/23/15 was fused to YFP^N, and IRT1 was fused to YFP^C. The PM marker was CBL1-OFP (g-TIP-mCherry). Different pairs of constructs were co-expressed in *N. benthamiana*. Scale bars, 40 μm. B, Fluorescence analysis of the location of the interaction between CPK21-nYFP and IRT1-cYFP in tobacco cells. The fluorescence intensity (mCherry/OFP and GFP signals) of the section lines was scanned using Fiji/ImageJ software. The location of the section line is marked in (A). C, LCI assay showing the interaction between CPK21/CPK23/CPK15 and IRT1. IRT1-cLUC/GUS-nLUC, GUS-cLUC/CPK21/23/15-nLUC, and GUS-cLUC/GUS-nLUC were used as negative controls. D, Pull-down assay showing the interaction between CPK21/CPK23/CPK15 and IRT1. IRT1vr was fused to GST and CPK21/CPK23/CPK15 to His. E, Co-immunoprecipitation of CPK21/CPK23 with IRT1 in IRT1-FLAG/CPK21-GFP and IRT1-FLAG/CPK23-GFP transgenic plants. The IRT1-FLAG/GFP, GUS-FLAG/CPK21-GFP, and GUS-FLAG/CPK23-GFP transgenic plants were used as negative controls.

teract directly with IRT1 *in vitro* and *in vivo*.

CPK21 and CPK23 primarily phosphorylate IRT1 at Ser149

CPKs are common protein kinases in plants that transmit Ca^{2+} signals downstream through the phosphorylation of various substrates and cause physiological responses (Kudla et al., 2018; Shi et al., 2018). We performed an *in vitro* kinase assay to detect whether CPK21 or CPK23 phosphorylated IRT1, and both kinases efficiently phosphorylated IRT1vr in these experiments (Figure 3A and C), suggesting that both intracellular fragments of IRT1 are phosphorylated by CPK21 and CPK23. The potential phosphorylation sites were searched using the prediction system network tool (http://gps.biocuckoo.cn/online.php). This method identified Ser149, Thr152, Ser153, Ser183, and Ser184 as potential CPK target residues. Next, we investigated the function of these potential sites by generating several IRT1 variants containing Ser(S) or Thr(T) point mutations to non-phosphodead Ala(A), including $IRT1vr^{S149A}$, $IRT1vr^{S152A}$, $IRT1vr^{S153A}$, $IRT1vr^{S183A}$, and $IRT1vr^{S184A}$. Subsequently, *in vitro* CPK21 and CPK23 phosphorylation assays were used to assess the extent of phosphorylation of these substrates. Phosphorylation analysis of IRT1vr revealed that IRT1vr-S149A phosphorylation was significantly attenuated compared with that of IRT1vr and that the IRT1 Ser149 site was a common primary target of CPK21/23 phosphorylation (Figure 3B and D). This finding further suggests the possibility of functional redundancy between CPK21/23.

To determine whether phosphorylation plays a potential regulatory role in IRT1 in Fe-deficient plants, we assessed whether the IRT1 phosphorylation level was affected by Fe-deficient conditions. Therefore, *Pro35S*:CPK21-FLAG transgenic plants were grown for 24 h under Fe-deficient conditions. The CPK21 protein was extracted and incubated with recombinant GST-IRT1vr purified from *E. coli* in the presence of [γ-^{32P}]ATP. The IRT1vr phosphorylation signals by CPK21 were significantly enhanced after 6 and 12 h of Fe deficiency (Figure 3E). To verify the ability of CPK21 kinase

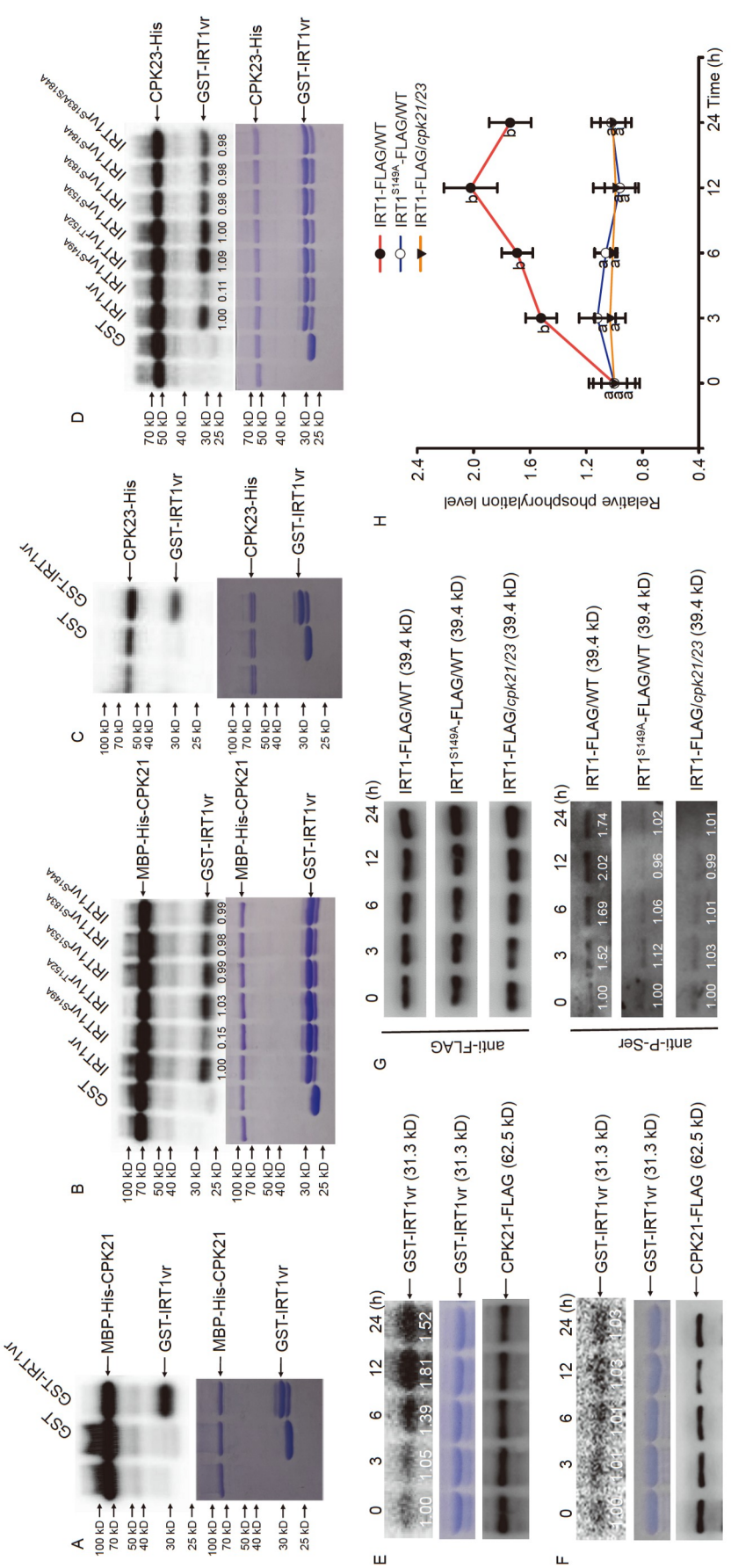

Figure 3 CPK21 and CPK23 phosphorylate IRT1 at Ser149. A, CPK21 phosphorylates IRT1vr *in vitro*. CPK21 was fused to MBP-His, whereas IRT1vr was fused to GST. B, Ser149 is essential for the phosphorylation of IRT1 by CPK21. CPK21 was fused to MBP-His, whereas the IRT1vr mutant variants were fused to GST. C, CPK23 phosphorylates IRT1vr *in vitro*. CPK23 was fused to His, whereas IRT1vr was fused to GST. D, Ser149 is essential for the phosphorylation of IRT1 by CPK23. CPK23 was fused to His, whereas the IRT1vr mutant variants were fused to GST. Top, autoradiograph; bottom, Coomassie Brilliant Blue (CBB) staining. E, CPK21 protein kinase assay with IRT1vr under Fe deficiency stress. Ten-day-old seedlings were treated with 300 μmol L^{-1} Ferrozine for the indicated times. F, CPK21 protein kinase assay with IRT1vr under Fe deficiency stress. Ten-day-old seedlings were treated with 300 μmol L^{-1} Ferrozine supplemented with 20 μmol L^{-1} $LaCl_3$ for the indicated times. The protein kinases were quantified by SDS-PAGE and are shown at the bottom. The IRT1vr phosphorylation signals caused by CPK21 were analyzed using ImageJ. Top, autoradiograph; middle, CBB staining; bottom, and Western blot image. G, Ten-day-old seedlings were treated under Fe-deficient conditions for 0, 3, 6, 12, and 24 h, respectively. The IRT1-FLAG protein was quantified by Western blot (top panel). The IRT1 and FLAG signals were detected with a P-Ser antibody and a FLAG antibody, respectively. H, The IRT1 phosphorylation signals were analyzed using ImageJ in (G).

to generate calcium signals under the Fe-deficient condition, *Pro35S*:CPK21-FLAG transgenic plants were transferred to Fe-deficient conditions and supplemented with 20 μmol L^{-1} $LaCl_3$ (a calcium channel blocker) for 24 h. We observed that the IRT1vr phosphorylation signals caused by CPK21 decreased significantly and that IRT1vr inducibility was almost lost at the same exposure time when Ca^{2+} signaling was absent (Figure 3F). These findings suggest that Ca^{2+} signaling is essential for phosphorylation by CPK21 and that the Fe-deficient conditions induced and persistently enhanced the ability of CPK21 to phosphorylate IRT1.

To explore whether the Fe-deficient sensitive phenotype of the *cpk21*/*23* mutant was related to the CPK activation-dependent phosphorylation state, we performed a timing and intensity analysis of Fe-deficient IRT1 phosphorylation. IRT1-FLAG/WT, IRT1-FLAG/*cpk21*/*23*, and $IRT1^{S149A}$-FLAG/WT transgenic plants were analyzed after 0, 3, 6, 12, and 24 h under Fe-deficient conditions. The results showed that the IRT1 phosphorylation level decreased in IRT1-FLAG/*cpk21*/*23* and $IRT1^{S149A}$-FLAG/WT plants compared with IRT1-FLAG/WT plants. The IRT1 phosphorylation level in IRT1-FLAG/WT was significantly enhanced after 3 h and peaked at 12 h. In contrast, IRT1-FLAG/*cpk21*/*23* and $IRT1^{S149A}$-FLAG/WT changed little. The timing and intensity of IRT1 phosphorylation were consistent with the observed activation of CPK21, which also started after 3 h under Fe-deficient conditions and peaked at 12 h (Figure 3G). These findings suggest that low Fe-induced Ser149 phosphorylation of IRT1 is dependent on CPK21/23 activity.

Phosphorylation of $IRT1^{S149}$ is essential for Fe transport activity rather than the localization and accumulation of IRT1

We performed a heterologous yeast complementation assay to determine the potential functional relevance of S149 phosphorylation. IRT1 and IRT1 Ser149 mutants were cloned into the pYES2 vector and expressed in WT yeast (BY4741) and the Δ*fet3fet4* yeast mutant (a low-Fe-sensitive yeast mutant) (Dix et al., 1994) on SD-U medium and SD-U supplemented with 80 μmol L^{-1} BPDS (chelates Fe ions) to determine the Fe transport function of IRT1 and whether changes had occurred (Khan et al., 2019). The results showed that IRT1 and $IRT1^{S149D}$ transported Fe through the PM and complemented the yeast Δ*fet3fet4* mutant, while the empty vector did not, and the point mutant $IRT1^{S149A}$ only weakly complemented the mutant (Figure 4A). Western blot analysis showed that the IRT1 protein levels in different yeast clones were similar (Figure S6A in Supporting Information).

We also performed a growth curve analysis using liquid cultures supplemented with 20 μmol L^{-1} BPDS to produce a Fe-deficient condition. The resulting growth trend was consistent with the above experimental results, where we found that the growth of Δ*fet3fet4* yeast containing an empty vector and the phosphodead variant $IRT1^{S149A}$ was restricted under Fe-deficient conditions (Figure 4C and D). To verify that the limited yeast growth was caused by Fe content, the yeast Fe content in liquid culture was determined by inductively-coupled plasma mass spectrometry (ICP-MS). As a result, the Fe content in yeast containing the empty vector or $IRT1^{S149A}$ was significantly lower than that in the other yeast strains (Figure 4B). Taken together, these results suggest that $IRT1^{S149A}$ phosphorylation affects the IRT1 Fe transport function. To explore whether a change in Ser149 affects Zn and Mn transport by IRT1, we performed heterologous yeast complementation assays using yeast Δ*smf1* (a low-Mn-sensitive yeast mutant) (Supek et al., 1996; Zhang et al., 2021a) and Δ*zrt1*/*zrt2* (a low-Zn-sensitive yeast mutant) (Eng et al., 1998; Martha-Paz et al., 2019). The results showed that changing the S149A residue did not change the ability of IRT1 to transport Mn or Zn (Figure S6C and D in Supporting Information).

To investigate whether changes in the phosphorylation sites would result in altered subcellular localization, we constructed respective fusion proteins containing the IRT1-GFP, $IRT1^{S149A}$-GFP, and $IRT1^{S149D}$-GFP fusion proteins under the control of the *IRT1* promoter. The expression vectors and fusion proteins were expressed in *irt1* or *irt1*/*cpk21*/*23* mutants. After 5 d of treatment under Fe-deficient conditions, IRT1 was expressed in the PM and cytoplasm of IRT1-GFP, $IRT1^{S149A}$-GFP, and $IRT1^{S149D}$-GFP transgenic plants, but no significant difference was detected between the Fe-sufficient and Fe-deficient conditions (Figure S7A and B in Supporting Information). This finding suggests that phosphorylation of CPK21/23 at Ser149 did not alter IRT1 localization. To rule out the case in which the IRT1-GFP fusion protein was not functional, thereby masking the changes in localization, we cloned the IRT1-GFP fusion DNA sequence in the pYES2 vector and expressed it in the Δ*fet3fet4* yeast mutant. The results showed that the yeast expressing the IRT1 protein did not differ in growth from the IRT1-GFP fusion protein, while the growth of the yeast expressing the $IRT1^{S149A}$-GFP fusion protein remained weak (Figure S7F in Supporting Information). In addition, Fe-deficient phenotype experiments were performed on *ProIRT1*:IRT1-GFP, *ProIRT1*:$IRT1^{S149}$A-GFP, and *ProIRT1*:$IRT1^{S149D}$-GFP transgenic plants. The results showed that IRT1-GFP and $IRT1^{S149D}$-GFP complemented the sensitive *irt1* mutant phenotype, whereas *ProIRT1*:$IRT1^{S149A}$-GFP was only partially complemented (Figure S7C–E in Supporting Information). These results show that the fusion of IRT1 with GFP did not affect the original function of IRT1 and that S149 phosphorylation did not affect the subcellular localization of IRT1 under Fe-deficient conditions.

To determine whether phosphorylation of IRT1 by CPK21/

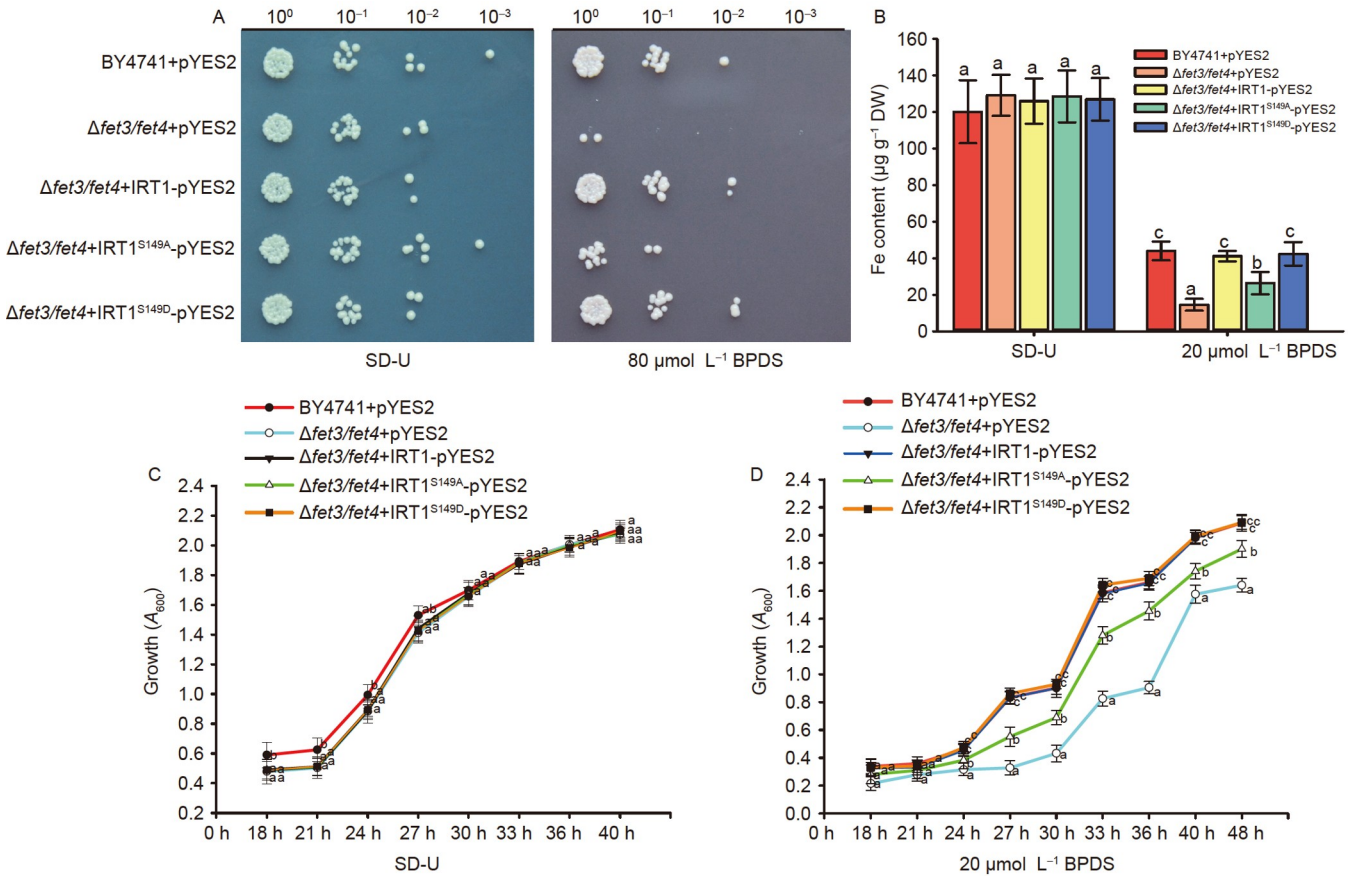

Figure 4 Functional analysis of IRT1^{S149} phosphorylation on Fe transport. A, Potential functional analysis of S149 phosphorylation in yeast. Growth of the yeast strains on normal medium (SD-U, lacking Ura) and treatment medium (SD-U+80 μmol L^{-1} BPDS) for 3–5 d. Four 10-fold dilution series were established under sterile conditions. B, Analysis of Fe content in yeast cells. Yeast cells grown in 20 μmol L^{-1} BPDS solution for 36 h were collected. C, Growth curves of yeast cells were plotted against the A_{600} values in the normal SD-U nutrient solution. The A_{600} values of yeast cell growth were monitored from 18 to 40 h. D, Growth curves of the yeast cells were plotted against A_{600} values in SD-U nutrient solution containing 20 μmol L^{-1} BPDS. The A_{600} values of yeast cell growth were monitored from 18 to 48 h. The data are mean±SD (n=3 biological replicates).

23 affected the accumulation of the IRT1 protein under Fe-deficient conditions, we performed an IRT1 Western blot analysis using a FLAG antibody. The IRT1-FLAG/WT and IRT1-FLAG/*cpk21*/*23* transgenic plants were grown for 7 d under Fe-sufficient conditions and then exposed to Fe-deficient conditions for 6 h. The results suggested that the accumulation of IRT1 was not affected regardless of the Fe conditions (Figure S8A and B in Supporting Information). To verify that the IRT1-FLAG fusion protein was functional in plants, we performed Fe-deficient phenotype experiments on the constructed IRT1-FLAG plants. The results showed that plants overexpressing the IRT1-FLAG fusion protein complemented the Fe deficiency sensitive phenotype observed in the *irt1* mutant and were tolerant of Fe deficiency compared with the WT plants, including increased root length (Figure S8C and D in Supporting Information). These results suggest that CPK21 and CPK23 phosphorylate IRT1^{ser149} specifically regulate the Fe transport activity of IRT1 rather than affect IRT1 abundance or localization.

To verify whether S149 phosphorylation plays a physiological role in plants, we generated the *irt1*/IRT1, *irt1*/IRT1^{S149A}, and *irt1*/IRT1^{S149D} transgenic lines under the control of the *IRT1* promoter and transformed the *irt1* mutant background. WT as well as *irt1*, *irt1*/IRT1, *irt1*/IRT1^{S149A}, and *irt1*/IRT1^{S149D} transgenic plants were cultured in Fe-sufficient and Fe-deficient medium for 10 d to observe the phenotypes. Transgenic lines with similar *IRT1* expression levels were used (Figure S6B in Supporting Information). Notably, the *IRT1 Fe* deficiency sensitive phenotype was completely restored in *irt1*/IRT1 plants. *irt1*/IRT1^{S149A} plants showed only partial rescue of the Fe deficiency sensitive *irt1* phenotype in terms of root length (Figure 5A and B), whereas *irt1*/IRT1^{S149D} plants exhibited increased root length (Figure 5C and D). These results suggest that other regulatory mechanisms may be in play. IRT1 S149 is not the only signal transduction regulatory site under Fe-deficient conditions, but phosphorylation of IRT1 S149 is critical for IRT1 to function properly in Fe-deficient conditions.

The Fe contents in roots and shoots of WT, *irt1*, *irt1*/IRT1, *irt1*/IRT1^{S149A}, and *irt1*/IRT1^{S149D} plants were calculated to

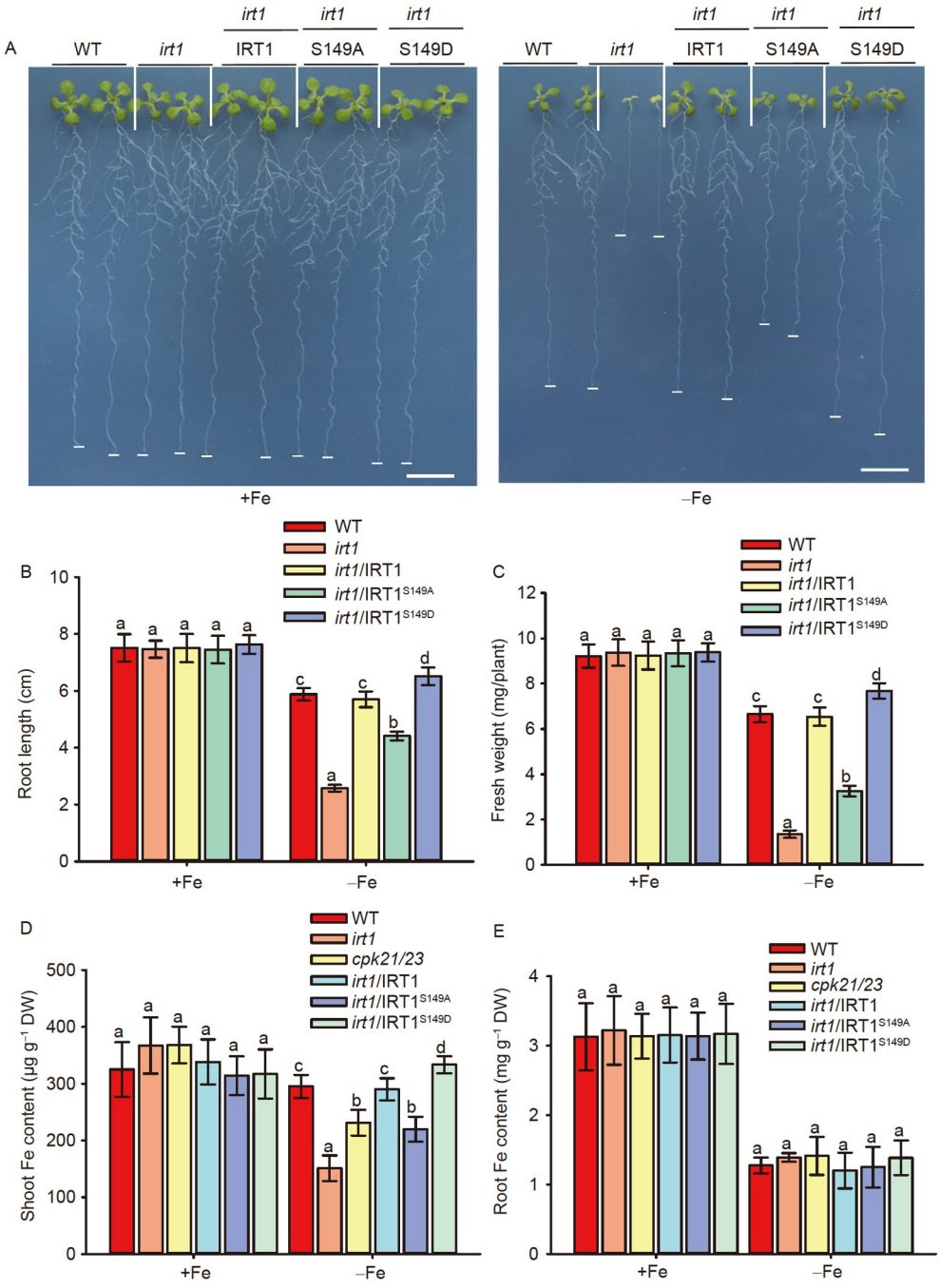

Figure 5 Functional analysis of IRT1 phosphorylated by CPK21/23 in plants. A, Fe-deficient phenotypes of the *irt1*/IRT1, *irt1*/IRT1^{S149A} and *irt1*/IRT1^{S149D} transgenic plants. Scale bars, 1 cm. B, Statistical analysis of the root lengths of the plants shown in (A). The data are presented as mean±SD (n=15 seedlings/genotype). C, Statistical analysis of the fresh weights of the plants shown in (A). The data are presented as mean±SD (n=15 seedlings/genotype). D, Analysis of the elemental content in the shoots. The data are mean±SD (n=3 biological replicates). E, Analysis of elemental content in the roots. The data are mean±SD (n=3 biological replicates).

determine the effect of regulating IRT1 on Fe homeostasis in plants through S149 phosphorylation transport activity. As a result, the Fe content of *cpk21/23* and *irt1*/IRT1^{S149A} plants decreased in shoots on a Fe-deficient medium, whereas the Fe content of *irt1*/IRT1^{S149D} plants increased in shoots. The Fe contents in roots and shoots of the *cpk21/23* and transgenic plants were not significantly different on the Fe-sufficient medium, compared with the WT (Figure 5E and F). These results further reinforced that Ser149 is a crucial phosphorylation site affecting IRT1 Fe transport activity and that the different phosphorylation states of the S149 residue have effects on growth and physiology.

CPK21 and CPK23 act upstream of IRT1

To explore the genetic interaction between CPK21, CPK23,

and IRT1, we crossed *CPK21-CA* and *CPK23-CA* with *irt1*. The growth phenotypes of the resulting lines were compared with those of the WT and *irt1* after growth on Fe-sufficient and Fe-deficient medium (Figure 6A and D). Specifically, under normal conditions, no differences were observed between the WT, *irt1*, *CPK21-CA*, *CPK23-CA*, *CPK21-CA*/*irt1*, and *CPK23-CA*/*irt1* plants, whereas the root lengths and fresh weights of *CPK21-CA*/*irt1* and *CPK23-CA*/*irt1* decreased significantly in the plants to an extent comparable to *irt1* plants under Fe-deficient conditions (Figure 6B, C, E, and F). All plants presented the same phenotype as the *irt1* mutant when *IRT1* was knocked out, regardless of whether *CPK21* and *CPK23* were overexpressed, indicating that CPK21/23 was upstream of the CPK21/23-IRT1 signaling pathway.

CPK21 and CPK23 do not affect ferric reductase activity or the rhizosphere acidification pathway

The key steps in Fe transport are rhizosphere acidification, ferric reductase activity, and IRT1-dependent Fe transport (Robinson et al., 1999; Santi and Schmidt, 2009; Vert et al., 2002). To determine whether CPK21/23 affects ferric reductase activity or the rhizosphere acidification signal pathway, we analyzed ferric chelate reductase activity and the pH of the rhizosphere in the *cpk21*/*23* mutant under +Fe/−Fe conditions. No significant differences in ferric reductase activity or rhizosphere acidification were detected in the *cpk21*/*23* mutant compared to the WT on Fe-sufficient and Fe-deficient medium (Figure S9A and B in Supporting Information). This result suggests that CPK21/23 responds to Fe-deficient conditions by regulating IRT1-dependent Fe transport rather than by affecting ferric reductase activity or the rhizosphere acidification pathway.

DISCUSSION

Fe is an essential trace element in plants, and a deficiency of Fe in the environment leads to fluctuations in Ca^{2+} concentrations in the root cytoplasm of *A. thaliana*, which generates Ca^{2+} signals (Gratz et al., 2019). In this study, we identified the CPK21/23-IRT1 signaling pathway, which regulates Fe transport under Fe-deficient conditions, and links Fe deficiency, Ca^{2+} signaling, and Fe transporters in *Arabidopsis*. We hypothesized that when plants sense Fe-deficient conditions, the spatiotemporal heterogeneity of the Ca^{2+} dynamics activates CPK21/CPK23, which, in turn, phosphorylate IRT1, thereby promoting the transport of Fe from the extracellular space to the intracellular space and enhancing tolerance to Fe deficiency (Figure 7).

CPK21/23 determines Fe homeostasis and tolerance to Fe deficiency in plants

Root growth is a developmental phenotype of plants that directly reflects the adaptability of plants to the growing conditions. IRT1 cannot transport sufficient Fe when plants are grown under Fe-deficient conditions; therefore, their growth and development are limited, which leads to differences in root length. Many studies have used root length as an indicator of plant adaptability, including IRT1, in terms of metal transport and calcium signal transduction (Dubeaux et al., 2018; Yang et al., 2019).

An important preliminary finding of our study is that the *cpk21*/*23* mutant was highly sensitive to Fe deficiency, whereas constitutively active CPK21 and CPK23 showed strong tolerance in transgenic plants. CPKs are Ca^{2+} sensors that play important roles in the responses to biotic and abiotic stressors by phosphorylating and modulating the activity of downstream substrates (Cheng et al., 2002; Kawamoto et al., 2015; Shi et al., 2018; Yip Delormel and Boudsocq, 2019). It has been reported that CPK21 and CPK23 are localized in the PM, where they play a crucial role in K^+ homeostasis and drought stress (Demir et al., 2013; Geiger et al., 2011; Ma and Wu, 2007; van Kleeff et al., 2018). In this study, CPK21/23 appeared to positively regulate tolerance to Fe-deficient conditions. We also observed that the *cpk21*/*23* double mutants exhibited a clear Fe deficiency sensitive phenotype, whereas the *cpk21* and *cpk23* single mutants did not. These findings suggest that the functions of CPK21 and CPK23 overlap to some extent in the regulation of Fe deficiency (Figure 1; Figures S1 and S2 in Supporting Information). The Fe content changed in the *cpk21*/*23* mutants (Figure 5). In addition, the CPK21 and IRT1vr protein kinase assay under Fe-deficient conditions showed that CPK21 kinase activity was induced by low Fe and peaked after 12 h. The significant upregulation of the *CPK21* and *CPK23* genes under Fe-deficient conditions also suggested that CPK21 and CPK23 respond to Fe deficiency signaling stress (Figure S3G in Supporting Information). These findings suggest that CPK21 and CPK23 play a critical role in Fe-deficient conditions.

CPK21/23 interacts with and phosphorylates the Fe transporter IRT1

The localization of CPK21 and CPK23 in the PM and the lack of a Fe-sensitive phenotype in the *cpk21*/*23* double mutant prompted us to consider the PM and intracellular-localized high-affinity Fe transporter IRT1 as a potential target for kinase regulation by these CPK proteins. IRT1 is a major Fe transporter that plays a key role in Fe absorption under Fe-deficient conditions in many plant species (including wheat, rice, and *Arabidopsis*) (Jiang et al., 2021; Lee and An, 2009; Vert et al., 2002). IRT belongs to the ZIP

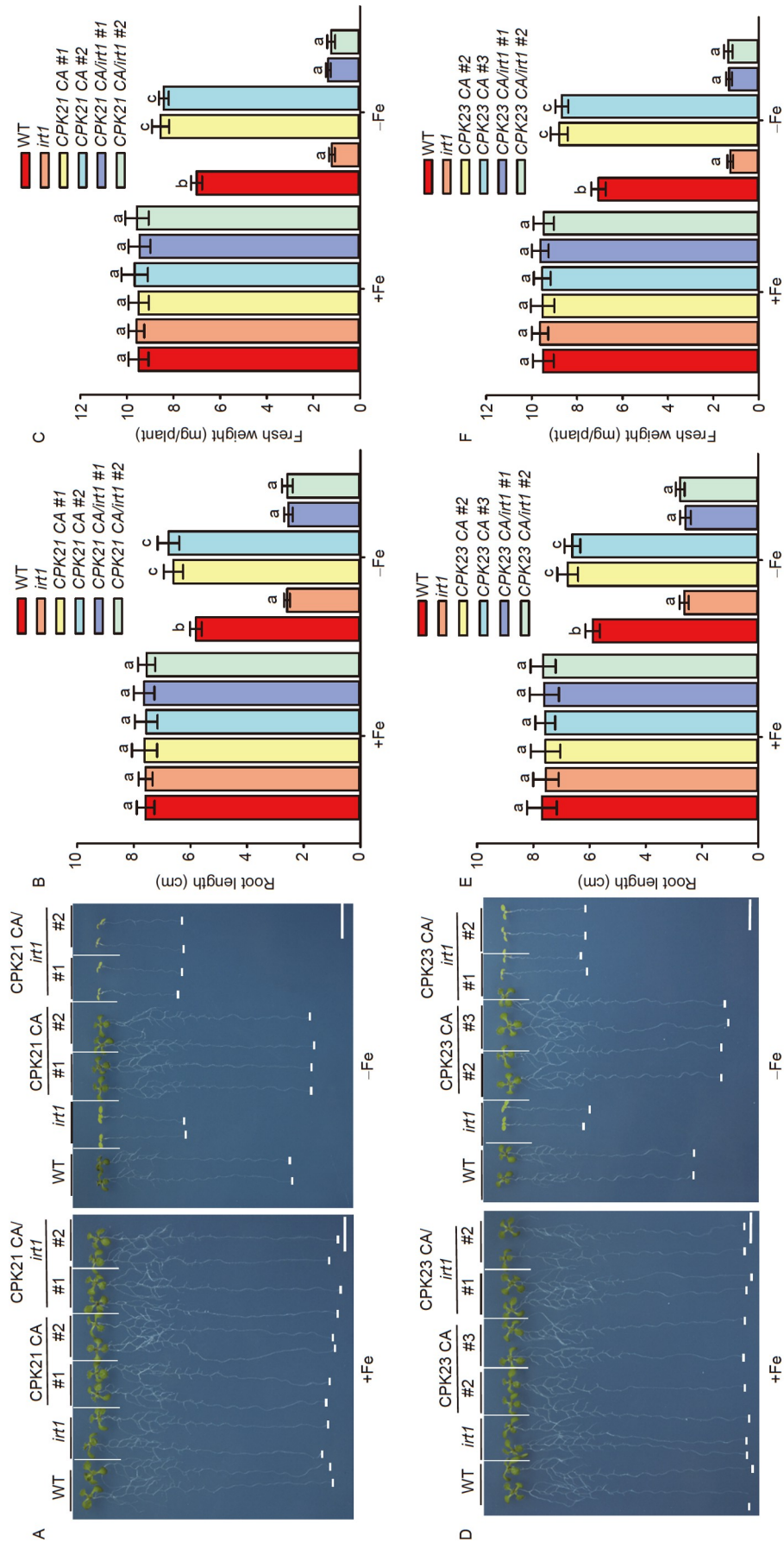

Figure 6 Genetic analysis of CPK21/CPK23 with IRT1. A, Fe deficiency phenotypes of the *CPK21-CA/irt1* transgenic plants. Scale bars, 1 cm. B, Statistical analysis of the root lengths of the plants shown in (A). C, Statistical analysis of the fresh weights of the plants shown in (A). D, Fe deficiency phenotypes of the *CPK23-CA/irt1* transgenic plants. Scale bars, 1 cm. E, Statistical analysis of the root lengths of the plants shown in (D). F, Statistical analysis of the root lengths of the plants shown in (D). The data are presented as mean±SD (n=15 seedlings/genotype).

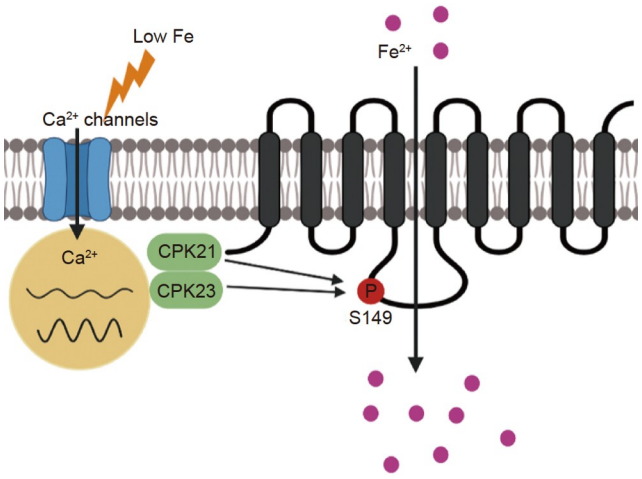

Figure 7 Fe deficiency signaling model and regulation of Fe transport by IRT1 in *Arabidopsis*. Ca^{2+} transport is promoted from the extracellular space to the intracellular space via Ca^{2+} channels when plants perceive a Fe deficiency in the environment. The spatiotemporal heterogeneity of the intracellular Ca^{2+} concentration generates unique Ca^{2+} signals. These physical parameters of Ca^{2+} signaling provide specific and critical information for triggering downstream responses. As important calcium regulatory proteins, CPK21 and CPK23 interpret the calcium signals triggered by Fe deficiency and decode the Ca^{2+} signals into protein phosphorylation, namely, Ser149 phosphorylation of the Fe transporter IRT1. Phosphorylated IRT1 is activated to further promote iron transport. This process consists of Ca^{2+} signaling, Ca^{2+}-CPK21-IRT1, and Ca^{2+}-CPK23-IRT1 axes, allowing for proper fine-tuning of plant Fe transport and homeostasis under Fe-deficient conditions.

protein family (Guerinot, 2000). When *Arabidopsis IRT1* was first discovered and cloned, it was expressed in Fe-deficient roots and was strictly regulated at the transcriptional and post-transcriptional levels (Conte and Walker, 2011; Eide et al., 1996; Vert et al., 2002). Indeed, the combined results of our interaction analysis identified the Fe transporter IRT1 as the primary target of the Fe deficiency pathway regulated by CPK21 and CPK23. We also found that CPK21 and CPK23 mainly phosphorylated IRT1 at Ser149 (Figures 2 and 3). The combined results of our phenotypic analysis using *irt1* mutation complementation with phosphomimetic and phosphodead IRT1 and our Fe content analysis supported the conclusion that phosphodead Ser149 in IRT1 significantly reduced IRT1 transport activity (Figure 5).

Western blot analysis of the IRT1-FLAG/WT and IRT1-FLAG/*cpk21/23* transgenic lines showed that the phosphorylation status of IRT1 did not affect protein accumulation. The Fe-deficient phenotypic analysis suggested the reliability of the plant materials (Figure S8 in Supporting Information). The localization of the IRT1Ser149A-GFP/*irt1*, IRT1Ser149D-GFP/*irt1*, and IRT1-GFP/*irt1*/*cpk21*/*23* in *Arabidopsis* root tip epidermal cells were not significantly different from that of IRT1-GFP/*irt1* (Figure S7 in Supporting Information). This finding supports that phosphorylation of CPK21 and CPK23 at Ser149 does not affect the subcellular localization of IRT1, reinforcing the conclusion that phosphorylation of IRT1 Ser149 is a key mechanism that regulates IRT1 transport activity and cellular Fe homeostasis.

Notably, a recent report showed that the phosphorylation of CPK21 and CPK23 regulates Thr498 of the Mn transporter NRAMP1 under Mn-deficient conditions and promotes Mn transport by NRAMP1 (Fu et al., 2022). However, phosphorylation of NRAMP1 at Thr498 does not alter its effect on Fe transport capacity under Fe-deficient conditions. Combining these findings with the results of the present study suggested that the regulation of IRT1 and NRAMP1 by CPK21 and CPK23 under specific conditions is independently regulated, and the two signaling pathways do not overlap. This independence seems to be the result of different conditions triggering different cytoplasmic Ca^{2+} signals to exhibit spatiotemporal heterogeneity, while CPK21 and CPK23 exercise different functions upon receiving different Ca^{2+} signals. CPK21 and CPK23 perform different functions in response to different Ca^{2+} signals. For example, the CPK21 and CPK23 responses to various abiotic stressors, such as ABA/drought stress (Geiger et al., 2011; Geiger et al., 2010; Mori et al., 2006). In addition, regulation of the CIPK23 protein kinase on IRT1 also occurs under −Fe conditions and in the presence of 10-fold higher Mn, Zn, and Co levels, while CIPK23 does not have that regulatory ability under Fe-deficient conditions (Dubeaux et al., 2018). Our analysis of the hybrid *cpk21*/*23*/*cipk23* mutant phenotype also indicated that *CIPK23* and *CPK21*/*23* independently regulate IRT1 under different conditions (Figure S10A and C in Supporting Information). Moreover, *the in vitro* kinase experiment revealed that the phosphorylation signal was not significantly weakened after the Ser149 mutation to alanine (A), indicating that CIPK23 did not phosphorylate IRT1 Ser149 (Figure S10E in Supporting Information). These studies reflected that CPKs or CIPKs perform different functions after receiving Ca^{2+} signals triggered by different stimuli.

Protein phosphorylation is a common mechanism of regulation and plays important roles in cell signal transduction (Liang and Zhou, 2018), such as in the physical interactions, phosphorylation, and activation of GUARD CELL HYDROGEN PEROXIDE-RESISTANT1 (GHR1) and the S-type ion channel SLOW ANION CHANNEL-ASSOCIATED1 (SLAC1) (Hua et al., 2012). Under high-salt stress, CBL-interacting protein kinase (CIPK) SOS2/CIPK24 phosphorylates and activates the Na^+/H^+ antiporter protein SOS1 on the PM to optimize tolerance to salt stress (Steinhorst et al., 2022). This study will guide our future research, and the results have improved our understanding of the mechanism through which calcium signaling regulates Fe homeostasis. The results also provide targets for developing crops resistant to Fe-deficient conditions.

MATERIALS AND METHODS

Plant materials and growth conditions

The WT plants used in this study were Columbia (Col-0) background. The T-DNA insertion lines *CPKs* and *irt1* (SALK_066735) were obtained from Nottingham Arabidopsis Stock Center. The mutants used are listed in Tables S1 and S2 in Supporting Information. The *Arabidopsis* seeds were grown on a nutrient medium consisting of 1% agar (Sigma-Aldrich, USA), 1% sucrose, and full strength Hoagland's nutrient solution (5 mmol L^{-1} $CaNO_3$, 5 mmol L^{-1} KNO_3, 2 mmol L^{-1} $MgSO_4$, 1 mmol L^{-1} $NH_4H_2PO_4$, 3 μmol L^{-1} H_3BO_3, 1 μmol L^{-1} $(NH_4)_6Mo_7O_{24}$, 0.4 μmol L^{-1} $ZnSO_4$, 0.2 μmol L^{-1} $CuSO_4$, 50 μmol L^{-1} Fe(III)-EDTA, pH 5.70) and −Fe medium (full strength Hoagland's nutrient solution without Fe(III)-EDTA), grown on vertical plates at 21°C for 10 d under a 16 h light/8 h dark cycle (Gao et al., 2018). All phenotypic experiments were repeated three times (n=15 for each genotype), and root length was measured using ImageJ (1.46r).

Plasmid construction

To construct the overexpression vector, the CDSs of the target genes were fused to the *Pro35S*:pCAMBIA-1307FLAG vector by homologous recombination (Manishankar et al., 2018), with the FLAG tag following the CDS. The 1,300 bp *IRT1* promoter and 1,237 bp genomic sequence were fused to the pCAMBIA-1300 vector for the genetic complementation analysis. Mutagenesis of $IRT1^{S149A}$ and $IRT1^{S149D}$ was performed using the Tiangen Rapid Site-Directed Mutagenesis Kit (Tiangen, Beijing, China).

The *CPK21* and *CPK23* CDSs were cloned into the *Pro35S*:nYFP and *Pro35S*:pCAMBIA 1300-nLUC vectors, respectively, for the BiFC and LCI analyses. The IRT1 CDS was cloned into the *Pro35S*:cYFP and *Pro35S*:pCAMBIA 1300-cLUC vectors, respectively (Su et al., 2021). The nYFP/cYFP/nLUC/cLUC labels all preceded the CDS.

To construct the recombinant protein vectors, *CPK21*, *CPK23*, and *IRT1*vr were amplified and cloned into the pET28a and pGEX4T-1 vectors to obtain CPK21/23-His and GST-IRT1vr. MBP-His-CPK21 was amplified and cloned into an engineered pMALc2X vector (His tag was added to the pMALc2X vector) to obtain MBP-His-CPK21. The GST or His-MBP tag preceded the CDS, while the His tag followed the CDS (Chen et al., 2021).

The promoter fragment and full-length CPK21/CPK23/IRT1 CDSs were cloned into the pCAMBIA-1300GFP vector to generate the *ProCPK21:*CPK21-GFP, *ProCPK23:*CPK23-GFP, and *ProIRT1:*IRT1-GFP constructs using the EcoRI and HindIII sites for the subcellular *Arabidopsis* localization analysis.

Semi-quantitative RT-PCR and quantitative real-time RT-PCR

Plant total RNA was extracted from 10-day-old seedlings using an RNA simple total RNA kit (Tiangen), and first-strand cDNA was synthesized from total RNA with the HiScript II Q RT SuperMix for qPCR (+gDNA wiper) (Vazyme, Shanghai, China), and the HiScript II 1st Strand cDNA Synthesis Kit (+gDNA wiper) for semi-quantitative RT-PCR (Vazyme). RT-qPCR was performed according to the instructions provided with the real-time PCR instrument (CFX connect, Bio-Rad, USA) using the ChamQ SYBR qPCR Master Mix (Vazyme). Statistical differences between the samples were evaluated by analysis of variance (ANOVA). The specific primers used are listed in Table S3 in Supporting Information.

BiFC assay

The BiFC assay was based on a published method (Su et al., 2021). In brief, a buffer was used to adjust the concentration of the *Agrobacterium tumefaciens* strain to a specific absorbance (A) at 600 nm. The combination of CPK21/23/15-nYFP and IRT1-cYFP, CPK21/23/15-nYFP and GUS-cYFP, IRT1-cYFP, and GUS-nYFP was injected into the leaves of *N. benthamiana* respectively. After 48 h of expression, the fluorescence signals were detected under a confocal laser scanning microscope (Olympus, Japan).

LCI assay

The LCI assay was based on a published method (Su et al., 2021). In brief, *A. tumefaciens* containing the CPK21/23/15-nLUC and IRT1-cLUC, the CPK21/23/15-nLUC and GUS-cLUC, the IRT1-cLUC and GUS-nLUC combinations were co-injected into *N. benthamiana* leaves, respectively. After 48 h of expression, the LCI signals were detected by a cooled charge-coupled device (Princeton, USA).

GST pull-down assay

The GST pull-down assay was based on a published method (Zhang et al., 2016). In brief, 3 μg of purified GST or GST-IRT1vr protein and glutathione beads (Sangon Biotech, Beijing, China) were incubated for 2 h. Then, they were incubated with 1 μg of CPK21/23/15-His for more than 2 h. After washing six times, the proteins were analyzed with anti-GST and anti-His antibodies (TransGen Biotech, Shanghai, China).

Protein purification and Western blot

The bacterial solution to extract *the E. coli* protein was induced overnight with IPTG, and the cell walls were broken

ultrasonically. The supernatant was obtained by centrifugation and passed through agarose beads with the corresponding label. The target protein was eluted and collected with the corresponding elution buffer (100 mmol L^{-1} reduced L-glutathione or 200 mmol L^{-1} imidazole in PBS). GST Settled Resin (Sangon Biotech) or Ni-NTA 6FF Settled Resin (Sangon Biotech) agarose beads were used for protein purification. To extract the plant proteins, the ground samples were added to the IP buffer and left to stand for 1 h (Ju et al., 2022). The supernatant was centrifuged, and the polyclonal antibody corresponding to the label was added to the supernatant. After more than 2 h of rotation, agarose coagulation beads were added and rotated for more than 2 h. Finally, the target protein was eluted and collected with the corresponding elution buffer.

After the target protein was extracted, the protein loading buffer was added to the sample, and the protein was denatured by heating at 95°C for 10 min. The samples were subjected to sodium dodecyl sulfate-polyacrylamide gel electrophoresis (SDS-PAGE). PVDF membranes were cut to a suitable size, and the proteins were transferred at a constant current of 200 mA for 2 h. The membranes were incubated with 5% nonfat dry milk for 2 h, and an appropriate primary/secondary antibody was added for 2 h. Finally, images were obtained using a chemiluminescence imager (Cell Signaling Technology, USA). The following antibodies were used to detect the proteins: anti-GFP (TransGen Biotech, 1:5,000), anti-FLAG (TransGen Biotech, 1:5,000), anti-His (TransGen Biotech, 1:5,000), anti-GST (TransGen Biotech, 1:5,000), anti-tubulin (TransGen Biotech, 1:5,000), and anti-phosphoserine (Immuno Way Biotechnology, USA; 1:2,000).

Co-IP assay

The Co-IP assay was based on a published method (Su et al., 2021). The total protein of 10-day-old transgenic seedlings was extracted with IP buffer. The extracts were incubated with GFP-tagged rabbit polyclonal antibody (Proteintech, USA) for 12 h at 4°C. Then, the proteins were incubated with protein A/G agarose beads (Abmart, USA) for 2 h at 4°C. The proteins were detected with anti-GFP (TransGen Biotech, 1:5,000) and anti-FLAG (TransGen Biotech, 1:5,000) antibodies.

In vitro and *in vivo* kinase assays

The *in vitro* kinase assay was based on a published method (Zhang et al., 2021b). IRT1-FLAG and IRT1^{S149A}-FLAG constructs were transformed into the WT or *cpk21*/*23* mediated by *A*. *tumefaciens* for the *in vivo* kinase assay. The seedlings were subjected to Fe-deficient conditions for 0, 3, 6, 12, and 24 h. The proteins were extracted and enriched with anti-FLAG agarose beads (Proteintech). The phosphorylation signals were analyzed by Western blot using a phosphoserine antibody (Immuno Way Biotechnology).

IRT1 subcellular localization

Using T3 stable lines of IRT1-GFP transgenic plants and their variants, GFP fluorescence was observed under confocal microscopy (Olympus) after vertical growth for 5 d in Fe-sufficient and Fe-deficient media. The excitation wavelength was 488 nm, and the emission wavelength was 500–530 nm. The PM:intracellular signal ratio was analyzed with ImageJ.

GUS expression analysis

ProIRT1:GUS, *ProCPK21:GUS*, and *ProCPK23:GUS* seedlings were grown under −Fe/+Fe conditions for 7 d and then stained using a GUS Staining Kit (Coolaber, Beijing, China). Chlorophyll was removed with an ethanol gradient (20%, 50%, and 70%). The samples were observed under a microscope (Olympus).

Yeast functional analysis

Yeast vectors expressing IRT1 and its variants were transformed into the Δ*fet3fet4*, Δ*smf1*, and Δ*zrt1*/*zrt2* yeast strains, respectively. SD-U liquid medium was used to culture the yeast grown to A=0.1. Four 10-fold dilution series were established under sterile conditions. The A_{600} values of the transgenic yeast were recorded every 3 h after 18 h of growth with 0 or 20 μmol L^{-1} BPDS to prepare the growth curve.

Elemental analysis

Seeds of WT, *irt1*, *cpk21*/*23*, *irt1*/IRT1, *irt1*/IRT1^{S149A}, and *irt1*/IRT1^{S149D} plants were sown on +Fe medium for 10 d, and the transgenic lines were transferred to Fe-sufficient or Fe-deficient medium for 5 d. The tissues were desorbed by washing in 2 mmol L^{-1} $CaSO_4$ and 10 mmol L^{-1} EDTA for 5 min, followed by a 10 min rinse in ddH_2O. The samples were dried at 65°C for 1 week. The plant samples and 5 mL of nitric acid were added to a digestion tube for mineralization, and digestion was carried out at 120°C for 5 h. Subsequently, 2 mL of ddH_2O_2 was added to the digestion tube in two portions, and the temperature was maintained. Then, the temperature was raised to 160°C and maintained until the nitric acid was completely volatilized. Finally, the samples were diluted with ddH_2O and analyzed by ICP-MS.

Ferric reductase assay

The ferric reductase assay was based on a published method

(Waters et al., 2006). In brief, the seedlings were grown on a Fe-sufficient medium for 10 d and transferred to a Fe-deficient medium for 0, 6, 12, 24, and 48 h. The absorbance value of the solution was measured at 562 nm using an ultraviolet/visible spectrophotometer (Shimadzu, Japan), and the liquid on the surface of the seedling was quickly dried, and the seedling was weighed.

Rhizosphere acidification assay

The rhizosphere acidification assay was based on a published method (Santi and Schmidt, 2009). In brief, 7-day-old seedlings were transferred to a standard nutrient solution containing +Fe or −Fe (0.005% bromocresol purple, pH 5.8). After a 48 h incubation in the test solution, the absorbance value of the solution was measured at 590 nm with an ultraviolet/visible spectrophotometer (Shimadzu) and then converted to pH according to the pH curve.

Statistical analysis

Statistical differences were identified by one-way ANOVA. Tukey's multiple-testing method ($P<0.05$) was used to detect the genotypes within a given growth condition (+Fe or −Fe). Three independent replicates were used for the plate experiments, confocal microscope experiments, qRT-PCR analysis, LCI, pull-down, functional analysis in yeast, and the Western blot assay, and a representative image was shown. Two independent replicates were assessed for the *in vitro* and *in vivo* protein kinase assays.

Compliance and ethics *The author(s) declare that they have no conflict of interest.*

Acknowledgements *This work was supported by the National Natural Science Foundation of China (32222008, 32100215, 31900236), Northwest A&F University (Z111021604), the open funds of China Postdoctoral Science Foundation (2018M643740), and Natural Science Basic Research Plan in Shaanxi Province of China (2019JQ-150). We thank Dr. Chao-feng Huang (National Key Laboratory of Plant Molecular Genetics) for yeast strain Δfet3/fet4, Dr. Hua Zhao, Dr. Xue-ling Huang and Feng-ping Yuan (State Key Laboratory of Crop Stress Biology in Arid Areas) for providing Olympus IX83-FV3000, CFX connect, and other platforms, Dr. Xiao-han Li (College of Natural Resources and Environment, Northwest A&F University) for providing technical support with ICP-MS.*

References

Barberon, M., Dubeaux, G., Kolb, C., Isono, E., Zelazny, E., and Vert, G. (2014). Polarization of IRON-REGULATED TRANSPORTER 1 (IRT1) to the plant-soil interface plays crucial role in metal homeostasis. Proc Natl Acad Sci USA 111, 8293–8298.

Barberon, M., Zelazny, E., Robert, S., Conéjéro, G., Curie, C., Friml, J., and Vert, G. (2011). Monoubiquitin-dependent endocytosis of the iron-regulated transporter 1 (IRT1) transporter controls iron uptake in plants. Proc Natl Acad Sci USA 108, E450–458.

Boudsocq, M., and Sheen, J. (2013). CDPKs in immune and stress signaling. Trends Plant Sci 18, 30–40.

Brandt, B., Brodsky, D.E., Xue, S., Negi, J., Iba, K., Kangasjärvi, J., Ghassemian, M., Stephan, A.B., Hu, H., and Schroeder, J.I. (2012). Reconstitution of abscisic acid activation of SLAC1 anion channel by CPK6 and OST1 kinases and branched ABI1 PP2C phosphatase action. Proc Natl Acad Sci USA 109, 10593–10598.

Briat, J.F., Fobis-Loisy, I., Grignon, N., Lobréaux, S., Pascal, N., Savino, G., Thoiron, S., Wirén, N., and Wuytswinkel, O. (1995). Cellular and molecular aspects of iron metabolism in plants. Biol Cell 84, 69–81.

Brumbarova, T., Bauer, P., and Ivanov, R. (2015). Molecular mechanisms governing *Arabidopsis* iron uptake. Trends Plant Sci 20, 124–133.

Chen, X., Ding, Y., Yang, Y., Song, C., Wang, B., Yang, S., Guo, Y., and Gong, Z. (2021). Protein kinases in plant responses to drought, salt, and cold stress. J Integr Plant Biol 63, 53–78.

Cheng, S.H., Willmann, M.R., Chen, H.C., and Sheen, J. (2002). Calcium signaling through protein kinases. The *Arabidopsis* calcium-dependent protein kinase gene family. Plant Physiol 129, 469–485.

Colangelo, E.P., and Guerinot, M.L. (2004). The essential basic helix-loop-helix protein FIT1 is required for the iron deficiency response. Plant Cell 16, 3400–3412.

Connolly, E.L., Fett, J.P., and Guerinot, M.L. (2002). Expression of the IRT1 metal transporter is controlled by metals at the levels of transcript and protein accumulation. Plant Cell 14, 1347–1357.

Conte, S.S., and Walker, E.L. (2011). Transporters contributing to iron trafficking in plants. Mol Plant 4, 464–476.

D'Angelo, C., Weinl, S., Batistic, O., Pandey, G.K., Cheong, Y.H., Schültke, S., Albrecht, V., Ehlert, B., Schulz, B., Harter, K., et al. (2006). Alternative complex formation of the Ca^{2+}-regulated protein kinase CIPK1 controls abscisic acid-dependent and independent stress responses in *Arabidopsis*. Plant J 48, 857–872.

Demir, F., Horntrich, C., Blachutzik, J.O., Scherzer, S., Reinders, Y., Kierszniowska, S., Schulze, W.X., Harms, G.S., Hedrich, R., Geiger, D., et al. (2013). *Arabidopsis* nanodomain-delimited ABA signaling pathway regulates the anion channel SLAH3. Proc Natl Acad Sci USA 110, 8296–8301.

Dix, D.R., Bridgham, J.T., Broderius, M.A., Byersdorfer, C.A., and Eide, D.J. (1994). The *FET4* gene encodes the low affinity Fe(II) transport protein of *Saccharomyces cerevisiae*. J Biol Chem 269, 26092–26099.

Dong, Q., Bai, B., Almutairi, B.O., and Kudla, J. (2021). Emerging roles of the CBL-CIPK calcium signaling network as key regulatory hub in plant nutrition. J Plant Physiol 257, 153335.

Dubeaux, G., Neveu, J., Zelazny, E., and Vert, G. (2018). Metal sensing by the IRT1 transporter-receptor orchestrates its own degradation and plant metal nutrition. Mol Cell 69, 953–964.e5.

Eide, D., Broderius, M., Fett, J., and Guerinot, M.L. (1996). A novel iron-regulated metal transporter from plants identified by functional expression in yeast. Proc Natl Acad Sci USA 93, 5624–5628.

Eng, B.H., Guerinot, M.L., Eide, D., and Saier Jr., M.H. (1998). Sequence analyses and phylogenetic characterization of the ZIP family of metal ion transport proteins. J Membr Biol 166, 1–7.

Franz, S., Ehlert, B., Liese, A., Kurth, J., Cazalé, A.C., and Romeis, T. (2011). Calcium-dependent protein kinase CPK21 functions in abiotic stress response in *Arabidopsis* thaliana. Mol Plant 4, 83–96.

Fu, D., Zhang, Z., Wallrad, L., Wang, Z., Höller, S., Ju, C.F., Schmitz-Thom, I., Huang, P., Wang, L., Peiter, E., et al. (2022). Ca^{2+}-dependent phosphorylation of NRAMP1 by CPK21 and CPK23 facilitates manganese uptake and homeostasis in *Arabidopsis*. Proc Natl Acad Sci USA 119, e2204574119.

Gao, H., Xie, W., Yang, C., Xu, J., Li, J., Wang, H., Chen, X., and Huang, C.F. (2018). NRAMP2, a *trans*-Golgi network-localized manganese transporter, is required for *Arabidopsis* root growth under manganese deficiency. New Phytol 217, 179–193.

Geiger, D., Maierhofer, T., AL-Rasheid, K.A.S., Scherzer, S., Mumm, P., Liese, A., Ache, P., Wellmann, C., Marten, I., Grill, E., et al. (2011). Stomatal closure by fast abscisic acid signaling is mediated by the guard cell anion channel SLAH3 and the receptor RCAR1. Sci Signal 4, ra32.

Geiger, D., Scherzer, S., Mumm, P., Marten, I., Ache, P., Matschi, S., Liese, A., Wellmann, C., Al-Rasheid, K.A.S., Grill, E., et al. (2010). Guard cell anion channel SLAC1 is regulated by CDPK protein kinases with distinct Ca^{2+} affinities. Proc Natl Acad Sci USA 107, 8023–8028.
Gratz, R., Manishankar, P., Ivanov, R., Köster, P., Mohr, I., Trofimov, K., Steinhorst, L., Meiser, J., Mai, H.J., Drerup, M., et al. (2019). CIPK11-dependent phosphorylation modulates FIT activity to promote *Arabidopsis* iron acquisition in response to calcium signaling. Dev Cell 48, 726–740.e10.
Gratz, R., von der Mark, C., Ivanov, R., and Brumbarova, T. (2021). Fe acquisition at the crossroad of calcium and reactive oxygen species signaling. Curr Opin Plant Biol 63, 102048.
Guerinot, M.L. (2000). The ZIP family of metal transporters. Biochim Biophys Acta 1465, 190–198.
Guerinot, M.L., and Yi, Y. (1994). Iron: nutritious, noxious, and not readily available. Plant Physiol 104, 815–820.
Gutermuth, T., Herbell, S., Lassig, R., Brosché, M., Romeis, T., Feijó, J.A., Hedrich, R., and Konrad, K.R. (2018). Tip-localized Ca^{2+}-permeable channels control pollen tube growth via kinase-dependent R- and S-type anion channel regulation. New Phytol 218, 1089–1105.
Hamel, L.P., Sheen, J., and Séguin, A. (2014). Ancient signals: comparative genomics of green plant CDPKs. Trends Plant Sci 19, 79–89.
Harmon, A.C., Gribskov, M., Gubrium, E., and Harper, J.F. (2001). The CDPK superfamily of protein kinases. New Phytol 151, 175–183.
Hashimoto, K., and Kudla, J. (2011). Calcium decoding mechanisms in plants. Biochimie 93, 2054–2059.
Hua, D., Wang, C., He, J., Liao, H., Duan, Y., Zhu, Z., Guo, Y., Chen, Z., and Gong, Z. (2012). A plasma membrane receptor kinase, GHR1, mediates abscisic acid- and hydrogen peroxide-regulated stomatal movement in *Arabidopsis*. Plant Cell 24, 2546–2561.
Ivanov, R., Brumbarova, T., and Bauer, P. (2012). Fitting into the harsh reality: regulation of iron-deficiency responses in dicotyledonous plants. Mol Plant 5, 27–42.
Ivanov, R., Brumbarova, T., Blum, A., Jantke, A.M., Fink-Straube, C., and Bauer, P. (2014). SORTING NEXIN1 is required for modulating the trafficking and stability of the *Arabidopsis* IRON-REGULATED TRANSPORTER1. Plant Cell 26, 1294–1307.
Jakoby, M., Wang, H.Y., Reidt, W., Weisshaar, B., and Bauer, P. (2004). *FRU* (*BHLH029*) is required for induction of iron mobilization genes in *Arabidopsis thaliana*. FEBS Lett 577, 528–534.
Jiang, Y., Chen, X., Chai, S., Sheng, H., Sha, L., Fan, X., Zeng, J., Kang, H., Zhang, H., Xiao, X., et al. (2021). TpIRT1 from Polish wheat (*Triticum polonicum* L.) enhances the accumulation of Fe, Mn, Co, and Cd in *Arabidopsis*. Plant Sci 312, 111058.
Ju, C., Zhang, Z., Deng, J., Miao, C., Wang, Z., Wallrad, L., Javed, L., Fu, D., Zhang, T., Kudla, J., et al. (2022). Ca^{2+}-dependent successive phosphorylation of vacuolar transporter MTP8 by CBL2/3-CIPK3/9/26 and CPK5 is critical for manganese homeostasis in *Arabidopsis*. Mol Plant 15, 419–437.
Kawamoto, N., Sasabe, M., Endo, M., Machida, Y., and Araki, T. (2015). Calcium-dependent protein kinases responsible for the phosphorylation of a bZIP transcription factor FD crucial for the florigen complex formation. Sci Rep 5, 8341.
Khan, I., Gratz, R., Denezhkin, P., Schott-Verdugo, S.N., Angrand, K., Genders, L., Basgaran, R.M., Fink-Straube, C., Brumbarova, T., Gohlke, H., et al. (2019). Calcium-promoted interaction between the C2-domain protein EHB1 and metal transporter IRT1 inhibits *Arabidopsis* iron acquisition. Plant Physiol 180, 1564–1581.
Kobayashi, T., and Nishizawa, N.K. (2012). Iron uptake, translocation, and regulation in higher plants. Annu Rev Plant Biol 63, 131–152.
Kudla, J., Becker, D., Grill, E., Hedrich, R., Hippler, M., Kummer, U., Parniske, M., Romeis, T., and Schumacher, K. (2018). Advances and current challenges in calcium signaling. New Phytol 218, 414–431.
Lee, S., and An, G. (2009). Over-expression of *OsIRT1* leads to increased iron and zinc accumulations in rice. Plant Cell Environ 32, 408–416.
Liang, X., and Zhou, J.M. (2018). Receptor-like cytoplasmic kinases: central players in plant receptor kinase-mediated signaling. Annu Rev Plant Biol 69, 267–299.
Lingam, S., Mohrbacher, J., Brumbarova, T., Potuschak, T., Fink-Straube, C., Blondet, E., Genschik, P., and Bauer, P. (2011). Interaction between the bHLH transcription factor FIT and ETHYLENE INSENSITIVE3/ETHYLENE INSENSITIVE3-LIKE1 reveals molecular linkage between the regulation of iron acquisition and ethylene signaling in *Arabidopsis*. Plant Cell 23, 1815–1829.
Liu, K.H., Niu, Y., Konishi, M., Wu, Y., Du, H., Sun Chung, H., Li, L., Boudsocq, M., McCormack, M., Maekawa, S., et al. (2017). Discovery of nitrate-CPK-NLP signalling in central nutrient-growth networks. Nature 545, 311–316.
Luan, S., and Wang, C. (2021). Calcium signaling mechanisms across kingdoms. Annu Rev Cell Dev Biol 37, 311–340.
Ma, S.Y., and Wu, W.H. (2007). AtCPK23 functions in *Arabidopsis* responses to drought and salt stresses. Plant Mol Biol 65, 511–518.
Manishankar, P., Wang, N., Köster, P., Alatar, A.A., and Kudla, J. (2018). Calcium signaling during salt stress and in the regulation of ion homeostasis. J Exp Bot 69, 4215–4226.
Marschner, H., and Römheld, V. (1994). Strategies of plants for acquisition of iron. Plant Soil 165, 261–274.
Martha-Paz, A.M., Eide, D., Mendoza-Cózatl, D., Castro-Guerrero, N.A., and Aréchiga-Carvajal, E.T. (2019). Zinc uptake in the Basidiomycota: characterization of zinc transporters in *Ustilago maydis*. Mol Membr Biol 35, 39–50.
Meiser, J., Lingam, S., and Bauer, P. (2011). Posttranslational regulation of the iron deficiency basic helix-loop-helix transcription factor FIT is affected by iron and nitric oxide. Plant Physiol 157, 2154–2166.
Mori, I.C., Murata, Y., Yang, Y., Munemasa, S., Wang, Y.F., Andreoli, S., Tiriac, H., Alonso, J.M., Harper, J.F., Ecker, J.R., et al. (2006). CDPKs CPK6 and CPK3 function in ABA regulation of guard cell S-type anion- and Ca^{2+} permeable channels and stomatal closure. PLoS Biol 4, 327–341.
Perochon, A., Aldon, D., Galaud, J.P., and Ranty, B. (2011). Calmodulin and calmodulin-like proteins in plant calcium signaling. Biochimie 93, 2048–2053.
Prodhan, M.Y., Munemasa, S., Nahar, M.N.E.N., Nakamura, Y., and Murata, Y. (2018). Guard cell salicylic acid signaling is integrated into abscisic acid signaling via the Ca^{2+}/CPK-dependent pathway. Plant Physiol 178, 441–450.
Robinson, N.J., Procter, C.M., Connolly, E.L., and Guerinot, M.L. (1999). A ferric-chelate reductase for iron uptake from soils. Nature 397, 694–697.
Santi, S., and Schmidt, W. (2009). Dissecting iron deficiency-induced proton extrusion in *Arabidopsis* roots. New Phytol 183, 1072–1084.
Scherzer, S., Maierhofer, T., Al-Rasheid, K.A.S., Geiger, D., and Hedrich, R. (2012). Multiple calcium-dependent kinases modulate ABA-activated guard cell anion channels. Mol Plant 5, 1409–1412.
Shi, S., Li, S., Asim, M., Mao, J., Xu, D., Ullah, Z., Liu, G., Wang, Q., and Liu, H. (2018). The *Arabidopsis* calcium-dependent protein kinases (CDPKs) and their roles in plant growth regulation and abiotic stress responses. Int J Mol Sci 19, 1900.
Shin, L.J., Lo, J.C., Chen, G.H., Callis, J., Fu, H., and Yeh, K.C. (2013). IRT1 DEGRADATION FACTOR1, a RING E3 ubiquitin ligase, regulates the degradation of IRON-REGULATED TRANSPORTER1 in *Arabidopsis*. Plant Cell 25, 3039–3051.
Steinhorst, L., He, G., Moore, L.K., Schültke, S., Schmitz-Thom, I., Cao, Y., Hashimoto, K., Andrés, Z., Piepenburg, K., Ragel, P., et al. (2022). A Ca^{2+} sensor switch for tolerance to elevated salt stress in *Arabidopsis*. Dev Cell 57, 2081–2094.e7.
Su, H., Wang, T., Ju, C., Deng, J., Zhang, T., Li, M., Tian, H., and Wang, C. (2021). Abscisic acid signaling negatively regulates nitrate uptake via phosphorylation of NRT1.1 by SnRK2s in *Arabidopsis*. J Integr Plant Biol 63, 597–610.
Supek, F., Supekova, L., Nelson, H., and Nelson, N. (1996). A yeast manganese transporter related to the macrophage protein involved in conferring resistance to mycobacteria. Proc Natl Acad Sci USA 93, 5105–5110.

Valmonte, G.R., Arthur, K., Higgins, C.M., and MacDiarmid, R.M. (2014). Calcium-dependent protein kinases in plants: evolution, expression and function. Plant Cell Physiol 55, 551–569.

van Kleeff, P.J.M., Gao, J., Mol, S., Zwart, N., Zhang, H., Li, K.W., and de Boer, A.H. (2018). The *Arabidopsis* GORK K^+-channel is phosphorylated by calcium-dependent protein kinase 21 (CPK21), which in turn is activated by 14-3-3 proteins. Plant Physiol Biochem 125, 219–231.

Vert, G., Grotz, N., Dédaldéchamp, F., Gaymard, F., Guerinot, M.L., Briat, J.F., and Curie, C. (2002). IRT1, an *Arabidopsis* transporter essential for iron uptake from the soil and for plant growth. Plant Cell 14, 1223–1233.

Wang, J.P., Xu, Y.P., Munyampundu, J.P., Liu, T.Y., and Cai, X.Z. (2016). Calcium-dependent protein kinase (CDPK) and CDPK-related kinase (CRK) gene families in tomato: genome-wide identification and functional analyses in disease resistance. Mol Genet Genomics 291, 661–676.

Waters, B.M., Chu, H.H., DiDonato, R.J., Roberts, L.A., Eisley, R.B., Lahner, B., Salt, D.E., and Walker, E.L. (2006). Mutations in Arabidopsis *Yellow Stripe-Like1* and *Yellow Stripe-Like3* reveal their roles in metal ion homeostasis and loading of metal ions in seeds. Plant Physiol 141, 1446–1458.

Wild, M., Davière, J.M., Regnault, T., Sakvarelidze-Achard, L., Carrera, E., Lopez Diaz, I., Cayrel, A., Dubeaux, G., Vert, G., and Achard, P. (2016). Tissue-specific regulation of gibberellin signaling fine-tunes *Arabidopsis* iron-deficiency responses. Dev Cell 37, 190–200.

Yang, Z., Wang, C., Xue, Y., Liu, X., Chen, S., Song, C.P., Yang, Y., and Guo, Y. (2019). Calcium-activated 14-3-3 proteins as a molecular switch in salt stress tolerance. Nat Commun 10, 1199.

Yip Delormel, T., and Boudsocq, M. (2019). Properties and functions of calcium-dependent protein kinases and their relatives in *Arabidopsis thaliana*. New Phytol 224, 585–604.

Zhang, B., Zhang, C., Liu, C., Fu, A., and Luan, S. (2021a). A Golgi-localized manganese transporter functions in pollen tube tip growth to control male fertility in *Arabidopsis*. Plant Commun 2, 100178.

Zhang, Z., Fu, D., Sun, Z., Ju, C., Miao, C., Wang, Z., Xie, D., Ma, L., Gong, Z., and Wang, C. (2021b). Tonoplast-associated calcium signaling regulates manganese homeostasis in *Arabidopsis*. Mol Plant 14, 805–819.

Zhang, Z., Hu, X., Zhang, Y., Miao, Z., Xie, C., Meng, X., Deng, J., Wen, J., Mysore, K.S., Frugier, F., et al. (2016). Opposing control by transcription factors MYB61 and MYB3 increases freezing tolerance by relieving C-repeat binding factor suppression. Plant Physiol 172, 1306–1323.

Zhou, L., Lan, W., Jiang, Y., Fang, W., and Luan, S. (2014). A calcium-dependent protein kinase interacts with and activates a calcium channel to regulate pollen tube growth. Mol Plant 7, 369–376.

Zhou, J., Wang, X., He, Y., Sang, T., Wang, P., Dai, S., Zhang, S., and Meng, X. (2020). Differential phosphorylation of the transcription factor WRKY33 by the protein kinases CPK5/CPK6 and MPK3/MPK6 cooperatively regulates camalexin biosynthesis in *Arabidopsis*. Plant Cell 32, 2621–2638.

Zhu, S.Y., Yu, X.C., Wang, X.J., Zhao, R., Li, Y., Fan, R.C., Shang, Y., Du, S.Y., Wang, X.F., Wu, F.Q., et al. (2007). Two calcium-dependent protein kinases, CPK4 and CPK11, regulate abscisic acid signal transduction in *Arabidopsis*. Plant Cell 19, 3019–3036.

SUPPORTING INFORMATION

The supporting information is available online at https://doi.org/10.1007/s11427-022-2330-4. The supporting materials are published as submitted, without typesetting or editing. The responsibility for scientific accuracy and content remains entirely with the authors.